Draft version March 15, 2007
Preprint typeset using LaTeX style emulateapj v. 12/01/06

NEAR-INFRARED PROPERTIES OF MODERATE-REDSHIFT GALAXY CLUSTERS: HALO OCCUPATION NUMBER, MASS-TO-LIGHT RATIOS AND Ω_M

Adam Muzzin
adam.muzzin@utoronto.ca
Dept. of Astronomy & Astrophysics, University of Toronto
50 St. George Street, Toronto, Ontario, Canada, M5S 3H4

H. K. C. Yee
hyee@astro.utoronto.ca
Dept. of Astronomy & Astrophysics, University of Toronto
50 St. George Street, Toronto, Ontario, Canada, M5S 3H4

Patrick B. Hall[1]
phall@yorku.ca
Department of Physics & Astronomy, York University
4700 Keele Street, Toronto, Ontario, Canada, M3J 1P3

H. Lin[1]
hlin@fnal.gov
Fermi National Accelerator Laboratory
P.O. Box 500, Batavia, IL 60510
Draft version March 15, 2007

ABSTRACT

Using K-band imaging for 15 of the Canadian Network for Observational Cosmology (CNOC1) clusters we examine the near-infrared properties of moderate-redshift ($0.19 < z < 0.55$) galaxy clusters. We find that the number of K-band selected cluster galaxies within R_{500} (the Halo Occupation Number, HON) is well-correlated with the the cluster dynamical mass (M_{500}) and X-ray Temperature (T_x); however, the intrinsic scatter in these scaling relations is 37% and 46% respectively. Comparison with clusters in the local universe shows that the HON-M_{500} relation does not evolve significantly between $z = 0$ and $z \sim 0.3$. This suggests that if dark matter halos are disrupted or undergo significant tidal-stripping in high-density regions as seen in numerical simulations, the stellar mass within the halos is tightly bound, and not removed during the process. The total K-band cluster light ($L_{200,K}$) and K-band selected richness (parameterized by $B_{gc,K}$) are also correlated with both the cluster T_x and M_{200}. The total (intrinsic) scatter in the $L_{200,K}$-M_{200} and $B_{gc,K}$-M_{200} relations are 43%(31%) and 35%(18%) respectively and indicates that for massive clusters both $L_{200,K}$ and $B_{gc,K}$ can predict M_{200} with similar accuracy as T_x, L_x or optical richness (B_{gc}). Examination of the mass-to-light ratios of the clusters shows that similar to local clusters, the K-band mass-to-light ratio is an increasing function of halo mass. Using the K-band mass-to-light ratios of the clusters, we apply the Oort technique and find $\Omega_{m,0} = 0.22 \pm 0.02$, which agrees well with recent combined concordance cosmology parameters, but, similar to previous cluster studies, is on the low-density end of preferred values.

Subject headings: cosmology: dark matter − large-scale structure of universe
galaxies: clusters: photometry − fundamental parameters

1. INTRODUCTION

One of the principal objectives in modern cosmology is a good description of the physics that govern the formation of structure from the galactic through to the supercluster scale. Recent theoretical and observational work in this area has concentrated on understanding the relationship between the dynamically dominant dark matter and the baryonic matter in the form of stars and gas. The major challenge has been that observables such as the galaxy correlation function (e.g., Zehavi et al. 2005a, 2005b; Eisenstein et al. 2005; Norberg et al. 2002, 2001), luminosity function (LF; e.g., Babbedge et al. 2006; Ilbert et al. 2005; Dahlen et al. 2005; Wolf et al. 2003; Blanton et al. 2003; Nakamura et al. 2003; Kochanek et al. 2001; Bell et al. 2003; Cole et al. 2001), and the Lyman-alpha forest (e.g., McDonald et al. 2006; Kim et al. 2002; Croft et al. 2002) constrain the distribution of stellar mass and gas in the universe, yet dark matter is the dominant gravitational component, and numerical simulations are more effective at predicting its distribution than that of baryonic mass..

Despite the difference between that which is easy to observe, and that which is easy to simulate, recent

[1] Visiting Astronomer, Kitt Peak National Observatory, National Optical Astronomy Observatory, which is operated by the Association of Universities for Research in Astronomy, Inc. (AURA) under cooperative agreement with the National Science Foundation.

combined N-body + Smoothed Particle Hydrodynamics (SPH) simulations have suggested that dissipation from the baryonic component is relatively unimportant in the process of galaxy formation because the force of gravity from galactic dark matter halos is overwhelmingly dominant (e.g., Weinberg et al. 2006; Nagai & Kravtsov 2005). These results naturally explain why purely N-body simulations have been able to reproduce the correlation function (e.g., Colín et al. 1999; Berlind & Weinberg 2002; Kravtsov et al. 2004; Tinker et al. 2005; Nagai & Kravtsov 2005; Tasitsiomi et al. 2004) and the number of satellite galaxies per halo, the Halo Occupation Number (HON) or its probability distribution, the Halo Occupation Distribution, (HOD, e.g., Berlind & Weinberg 2002, see Cooray & Sheth 2002 for a review). Furthermore, full SPH simulations (e.g., Weinberg et al. 2006, 2004; Yoshikawa et al. 2001; Pearce et al. 2001) and semi-analytic models (e.g., Berlind et al. 2005, 2003; Cole et al. 2000; Zhu et al. 2006) which can be directly compared to observations, have also begun to enjoy a great deal of success at reproducing the LF, correlation function, and HON. These recent improvements in the quality of simulations and semi-analytic models as well as new observational datasets such as the SDSS and 2dFRS represent a major breakthrough in our understanding of the relative distribution of baryonic and dark matter in the universe and consequently, the formation of large-scale structure.

Detailed studies of galaxy clusters offer a complementary approach to the correlation function, Lyman-alpha forest, and simulations for studying the relationship between baryonic and dark matter. Clusters allow us to probe the distribution of baryons and dark matter in the most massive collapsed halos (which also happen to be the best-resolved objects in numerical simulations). The advantage of studying clusters is that the baryonic content in the form of stars and hot gas in the Intra-Cluster Medium (ICM) can be directly measured with observations, and in addition to this, cluster halos are sufficiently massive that their dark matter mass can be measured using either weak lensing, X-ray data, or the dynamics of cluster galaxies. This allows direct comparison between the baryonic and non-baryonic component on a halo-by-halo basis, whereas for galaxy-mass halos, the mass-to-light ratio (M/L), HON, or bias is usually measured statistically using either galaxy-galaxy lensing (e.g., Seljak et al. 2005; Sheldon et al. 2004; Hoekstra et al. 2005, 2002), or by stacking galaxies and studying the dynamics of satellite galaxies (e.g., Conroy et al. 2005, Brainerd et al. 2003), although recently strong-lensing analysis of a sample of individual systems has been done (Treu et al. 2006). The advantage of being able to study individual halos is that not only can the correlation between baryonic and dark matter be measured (via the HON or M/L ratio), but the relative *scatter* in the correlation can also be determined. Good constraints on the scatter are important because it is a direct measure of the stochasticity in the baryonic/dark matter bias.

In practice, the best way to measure the baryonic content of clusters in the form of stars is with detailed modeling of the stellar populations using either high-resolution spectroscopy, or multi-band photometric observations. As these observations are often difficult to obtain for large samples of galaxies, K-band light has frequently been adopted as a cheap and efficient proxy for the stellar mass of galaxies. K-band light is neither strongly affected by dust, nor strongly enhanced by starbursts, and is therefore a good tracer of underlying stellar mass of a galaxy (e.g., Brinchmann & Ellis 2000; Gavazzi et al. 1996; Rix & Rieke 1993). Furthermore, k-corrections are generally small, and fairly independent of galaxy type (Poggianti 1997; Mannucci et al. 2001). Therefore, a study of the relative abundances of K-band light and mass in clusters is a good probe of the relationship between the cluster dark matter mass and the baryonic mass in the form of stars.

In addition to being useful for determining the relationship between dark matter and baryonic matter, a good understanding of the slope and scatter of the cluster K-band luminosity-mass correlation and K-band richness-mass correlation will be extremely valuable in the era of high-yield cluster surveys such as the Red-sequence Cluster Survey 2 (RCS-2, Yee et al. 2007), the South Pole Telescope (SPT, Ruhl et al. 2004), and the Atacama Cosmology Telescope (ACT, Kosowsky 2006). These projects will use the evolution of the cluster mass function, N(M, z) as a probe of cosmological parameters (see Mohr 2004 for a review); however, mass measurements for the thousands of clusters that will be detected in these surveys are unlikely to be available from traditional techniques such as L_x, T_x, weak-lensing, or dynamics and therefore new, observationally cheaper proxies for cluster mass will be required. Two candidates for this mass indicator are the integrated Sunyaev-Zeldovich Effect (SZE) y-parameter (e.g., Motl et al. 2005), as well as the total cluster K-band luminosity or K-band selected richness (e.g., L04, Ramella et al. 2004, Rines et al. 2004). For the SZE surveys the y-parameter has significant potential as a mass indicator (e.g., Hallman et al. 2006, Motl et al. 2005) as it is a measure of the mass of cluster baryons in the form of hot gas. For optical/IR surveys, K-band richness/luminosity is an attractive alternative because it is a measure of the total mass of baryons in the form of stars in cluster galaxies. Gladders et al. (2006) have already shown that optical richness works well as a cluster mass proxy, and using the optically-selected RCS-1 survey and an empirical mass-richness calibration they determined cosmological parameters consistent with recent concordance values (e.g., Spergel et al. 2006), thus illustrating the potential for this technique. K-band light is a better tracer of stellar mass than optical light, and therefore it might be expected that the scatter in the K-band light/richness vs. mass relation will be smaller than the scatter in the optical light/richness vs. mass relation, or at least might have fewer catastrophic outliers. Using an observable with a smaller scatter, and fewer outliers could improve the accuracy in the measured cluster mass function (e.g., Lima & Hu 2005).

Since the advent of the 2-Micron All Sky Survey (2MASS, Skrutskie et al. 2006) several studies of the relationship between K-band light and dark matter in local ($z < 0.1$) clusters have been done. Lin et al. (2003, 2004; hereafter L04), Rines et al. (2004), Kochanek et al. (2003), and Ramella et al. (2004) all show that the K-band selected number counts and total cluster K-band light are indeed correlated with the dark matter mass, and have rms scatters of $\sim 40\%$. L04, Rines et al. (2004), and Ramella et al. (2004) also show that the

slope of the L_K vs. M_{200} relation is shallower than unity for clusters, suggesting that the conversion of baryons into stellar mass proceeds less efficiently in higher-mass halos. Recently, Lin et al. (2006) presented an analysis of the K-band selected HON for a heterogeneous sample of 27 clusters at $0 < z < 0.9$ and found no significant evolution in the HON-Mass relation with redshift. Interestingly, this result was different from their original analysis using a subsample of ~ 20 clusters at $0.2 < z < 0.9$ where they found the HON at fixed mass increases by a factor of ~ 2 at $z > 0.2$.

The purpose of this paper is to extend the analysis of the local cluster K-band HON and M/L ratio to higher redshift using a well-defined sample of clusters with wide-field imaging and extensive spectroscopic data. Our sample consists of 15 massive, X-ray selected clusters that were part of the Canadian Network for Observational Cosmology (CNOC1, Yee et al. 1996) project. The K-band imaging, LF and density profiles for the clusters were presented in the first paper in this series (Muzzin et al. 2006, hereafter Paper I). In addition to the K-band imaging, these clusters also have considerable optical spectroscopy and g and r photometry both of which extend to $R \sim R_{200}$ for each cluster.

The structure of this paper is as follows: In §2 we briefly describe the dataset, and in §3 present updated values for the cluster dynamical masses and X-ray temperatures. In §4 we present the cluster HON and discuss its redshift evolution. Section 5 shows that total K-band luminosity ($L_{200,K}$) and K-band selected richness (parameterized by $B_{gc,K}$) are correlated with the cluster halo mass, and can potentially be used as cheap proxies for this quantity in cluster abundance surveys. In §6 we present the K-band M/L ratios for the CNOC1 clusters and in §7 we present a measurement of Ω_m using the Oort (1958) technique. We conclude with a summary in §8. When computing magnitudes and angular sizes we adopt an $\Omega_m = 0.3$, $\Omega_\Lambda = 0.7$, $H_0 = 70$ km s^{-1} Mpc $^{-1}$ cosmology.

2. DATA

The CNOC1 clusters are a set of 16 massive clusters with redshifts $0.17 < z < 0.54$. Fifteen of the clusters were detected in the Einstein Medium Sensitivity Survey (EMSS, Gioia et al. 1990). Abell 2390 was added as the 16th cluster and is also a massive cluster with strong X-ray emission. The clusters have extensive optical photometry and spectroscopy which were obtained as part of the CNOC1 project (Yee et al. 1996). Our sample is comprised of 15 of the 16 CNOC1 clusters. The cluster MS0906+11 is omitted because it was shown to be a strong binary in redshift-space by Carlberg et al. (1996) and therefore the mass measurement for the cluster is unreliable. The optical photometric and spectroscopic data as well as the K-band photometric data used in this paper were already presented in Paper I. We refer to that paper as well as the CNOC1 paper (Yee et al. 1996) for complete details of the observations, reductions and photometry and below present only a quick overview of the data.

2.1. *Optical Photometry and Spectroscopy*

Gunn g and r band imaging data were obtained at the 3.6m Canada-France-Hawaii-Telescope (CFHT) using the Multi-Object Spectrograph (MOS) camera. Photometry was performed on these data using the Picture Processing Package (PPP, Yee 1991). The photometry reaches a 5σ depth of $\sim M^* + 3$ in both the g and r bands. The CNOC1 collaboration also obtained > 2500 spectroscopic redshifts in the fields of the 15 clusters using the CFHTMOS. Of these, approximately one-half are cluster members. The spectroscopy is sparsely sampled, but complete to a depth of $K^* + 2$ for all but the two highest-redshift clusters (MS0016+16 and MS0451-03). The spectroscopy for those clusters is complete to $\sim K^* + 1$.

2.2. *Near Infrared Photometry*

K-band imaging for 14 of the 15 clusters was obtained at the Kitt Peak National Observatory (KPNO) 2.1m telescope using the Ohio State / NOAO Infrared Imaging Spectrograph (ONIS). Observations were taken in a Mauna Kea filter set version of the K_s filter (Tokunaga K), which is nearly identical to the 2MASS K_s filter. For our analysis we treat the Tokunaga K filter as the K_s-band and hereafter refer to it as the "K-band". K_s-band imaging of MS0440+02 was obtained using the PISCES camera on the Steward Observatory 90″ telescope. Photometry for the K-band data was also performed using PPP. The K-band imaging is complete to a 5σ depth of $\sim K^* + 2$ for all clusters, except the two highest-redshift clusters where it is complete to $\sim K^* + 1$ (see Table 1 of Paper I for a summary of observations).

3. CLUSTER PHYSICAL PARAMETERS

The masses of the CNOC1 clusters are without a doubt the most well-studied for clusters at moderate redshift. There are numerous measurements using X-ray temperatures (T_x, Hicks et al. 2006; Lewis et al. 1999; Henry 2000; Mushotzky & Scharf 1997), the dynamics of cluster galaxies (van der Marel et al. 2000; Borgani et al. 1999; Carlberg et al. 1996; 1997; Diaferio et al. 2005), and both strong (Fahlman et al. 1994; Luppino & Gioia 1995; Pierre et al. 1996, Wu 2000) and weak lensing (Allen 1998; Hoekstra et al. 1998; Smail et al 1995; 1997). In this section we discuss the masses and dynamical radii we adopt for comparing with the K-band properties.

3.1. *Dynamical Masses*

The first study of the dynamics of the CNOC1 clusters was done by Carlberg et al. (1996) who measured the line-of-sight velocity dispersion (σ_1) for each cluster. These velocity dispersions were used to calculate the virial mass (M_{vir}), the radius at which the cluster mass density exceeds the critical density of the universe by a factor of 200 (R_{200}), and the mass contained within that radius (M_{200}), by assuming the cluster had an isotropic velocity ellipsoid. In subsequent work, Carlberg et al. (1997) and van der Marel et al. (2000) examined in detail the velocity dispersion profiles, and velocity anisotropy of the clusters. van der Marel et al. (2000) verified that they are compatible with an isotropic velocity ellipsoid and that the cluster mass profile was consistent with an NFW (Navarro et al. 1997) profile. The cluster velocity dispersions were also determined by Borgani et al. (1999) using different background subtraction techniques. They found that the different techniques provide velocity dispersions that are self-similar to $\sim 10\%$, and that the

velocity dispersions they derive are also consistent to $\sim$ 10% with the Carlberg et al. (1997) velocity dispersions.

Unfortunately, the M_{200} and R_{200} values determined from these studies are now out of date because they were computed assuming cosmological parameters which are different from recent concordance values (e.g., Spergel et al. 2006). Fortunately, the velocity dispersions do not depend on cosmology and, given that the clusters are consistent with an isotropic velocity ellipsoid, we have recomputed both R_{200} and M_{200} with a $\Omega_m = 0.3$, $\Omega_\Lambda = 0.7$, $H_0 = 70$ km s^{-1} Mpc^{-1} cosmology using the equations,

$$R_{200} = \frac{\sqrt{3}\sigma_1}{10H(z)}, \quad (1)$$

and,

$$M_{200} = \frac{4}{3}\pi R_{200}^3 \cdot 200\rho_c, \quad (2)$$

where $H(z)$ is the Hubble constant at redshift z, and ρ_c is the critical density for a flat universe. Equation 1 can be derived by assuming $M_{200} \approx M_{vir}$ and equating the virial theorem ($M_{vir} = \frac{3}{G}\sigma_1^2 R_{vir}$) and Equation 2. For all clusters the σ_1 values determined by Carlberg et al. (1997) are used to compute M_{200} and R_{200}. Errors in M_{200} are calculated by propagating the errors in σ_1 in the standard way. The new values of R_{200} and M_{200} are on average $\sim$ 1.6 times larger than the Carlberg et al. (1997) values. We list the updated values in Table 1.

3.2. *X-ray Temperatures*

X-ray temperatures have been measured for the CNOC1 clusters by several authors. The clusters we originally discovered in the Einstein Medium Sensitivity Survey (EMSS, Gioia et al. 1990); however, only X-ray fluxes were computed using the original data. Subsequently, Lewis et al. (1999) measured T_x for 13 of the 15 clusters in our sample using data from the ROSAT satellite. They found that the average cluster masses determined from T_x were in good agreement with the updated dynamical masses, even though individual clusters could have discrepancies as large as a factor of 2. Recently, Hicks et al. (2006) used archival Chandra Advanced CCD Imaging Spectrometer (ACIS) data to determine accurate T_x values for 13 of the 15 clusters in our sample. They use single and double-β-model fits to determine the temperatures. Several clusters (A2390, MS0839+29, MS1358+62, MS1455+22) are also corrected for significant cooling flows. They find that the X-ray masses they compute agree well with the dynamical masses determined with the velocity dispersions of Carlberg et al. (1997) and Borgani et al. (1999). These new T_x values are superior to the older data and for comparisons with the HON (§4), $L_{200,K}$ (§5.1), and $B_{gc,K}$ (§5.2) we use these values. There are two clusters without a Chandra observation (MS1224+20, MS1231+15). For MS1224+20 we use the temperature listed in Lewis et al. (1999). MS1231+15 has no X-ray temperature available so we assume a temperature of 6 keV, which is appropriate given the X-ray luminosity (Yee & Ellingson 2003). We list the X-ray temperatures and their associated errors in Table 1.

4. THE HALO OCCUPATION NUMBER

Clusters are massive dark matter halos, and therefore computing their HON simply requires counting the total number of cluster members within some dynamical radius, typically R_{200}. The extensive spectroscopy for the CNOC1 clusters could be used to differentiate between field and cluster galaxies; however, we prefer to measure the HON using statistical background subtraction. Using spectroscopic data to separate field and cluster galaxies is preferable when computing cluster properties that depend on the luminosity of cluster members (e.g., LFs, total luminosity §5.1, or M/L ratios §6.1) because these calculations require information on the membership of individual galaxies to compute distance moduli and k-corrections. However, unless the spectroscopy of a cluster field is quite complete, statistical background subtraction is better-suited for counting the overdensity of cluster galaxies. Furthermore, using statistical background subtraction provides a consistent technique for each cluster and avoids any biases from cluster-to-cluster that might be caused by poor determination of the spectroscopic selection function.

The background counts are measured from our own K-band imaging survey of CNOC2 fields (Yee et al. 2000). The data was taken using the PISCES camera on the Steward Observatory 90″ telescope and are reduced and photometered using the same techniques as for the CNOC1 dataset. The imaging consists of 23 (8′ × 8′) fields and covers a total area of 0.26 square degrees. Complete details of the observations, data reduction, and photometry will be presented in a future paper (Lin et al. in preparation). Figure 1 shows background counts from the CNOC2 fields with the number counts from the K20 Survey (Cimatti et al. 2002) and the MUNICS Survey (Drory et al. 2001) overplotted for comparison. The CNOC2 galaxy counts agree well with the counts from these surveys as well as various other K-band surveys in the literature (e.g., Elston et al. 2006; Maihara et al. 2001; Saracco et al. 2001; Gardner et al. 1993).

We measure the HON for the clusters within the radius R_{500} (the radius at which the cluster mass density exceeds the critical density of the universe by a factor of 500), rather than the more typical R_{200}. It would be preferable to use R_{200}, as it is similar to the cluster virial radius; however, some of the clusters are very sparsely sampled at R_{200}, and therefore require large corrections to compensate for the poor sampling. These corrections propagate as large uncertainties in the total number of galaxies. Conversely, the coverage at R_{500} is complete for all clusters (except MS1455+22) and therefore those measurements have much smaller uncertainties and should also be more robust. The cluster R_{500} is estimated from the R_{200} values assuming an NFW profile with c = 5. Hereafter we refer to the HON within R_{500} as N_{500} and the HON within R_{200} as N_{200}.

Thus far, the largest study of the cluster HON is the work of L04 who measured N_{500} and N_{200} for 93, X-ray selected, $z < 0.1$ clusters using 2MASS data. In order to make a direct comparison between our sample and their sample, we measure N_{500} using the same limiting magnitude as L04. Their technique for measuring the HON involves determining the Schechter parameters K^* and ϕ^* for each cluster and then integrating the Schechter function to an absolute magnitude limit of M_K = -21 to find the total cluster counts. For their ensemble of 93

clusters, they measured K^* = -24.02 ± 0.02. Therefore, statistically speaking, their N_{500} values are measured at $K^* + 3$, although the depth varies from cluster-to-cluster. Our data does not reach $K^* + 3$ for most clusters, therefore galaxies are counted to $K^* + 1$ and then these counts are extrapolated to $K^* + 3$.

K^* evolves with redshift; however, we showed in Paper I that the evolution tightly follows the luminosity evolution of a single-burst population formed at high-redshift. The single-burst model from Paper I is used to infer K^* at the redshift of each cluster. The background subtracted, $K < K^* + 1$ counts are scaled to the appropriate counts for $K^* + 3$ by extrapolating a Schechter function with a faint-end slope of α = -0.9. This value of α is consistent with the faint-end slope measured for the CNOC1 cluster LF in Paper I (α = -0.84 ± 0.08) and is similar to the faint-end slope measured for the L04 data (α = -0.84 ± 0.02).

We plot N_{500} vs. M_{500} for the clusters in the left panel of Figure 2, and N_{500} vs. T_x in right panel of Figure 2. In both cases there is a good correlation between the two parameters. The Spearman rank-correlation coefficients are 0.79 and 0.77 respectively, implying probabilities of 7.1×10^{-4}, 8.5×10^{-4} that the data are uncorrelated.

One cluster which has an extremely small N_{500} for its mass is MS1455+22. This cluster is also a significant outlier in the M_{200}-B_{gc} relation (B_{gc} is a measure of cluster richness, see §5.2) from Yee & Ellingson (2003, hereafter YE03). They suggest that the most logical interpretation is either that the mass has been significantly overestimated or else that the cluster is in a very advanced state of evolution, different from most clusters in this redshift range. Therefore, MS1455+22 is excluded when we fit both M_{500} vs. N_{500} and and T_x vs. N_{500} and is plotted in Figure 2 as an open triangle. Using a χ^2-minimization technique for errors in both parameters (Press et al. 1992) we find the best-fit relation for the N_{500} - M_{500} correlation is

$$Log(M_{500}) = (1.40 \pm 0.22) Log(N_{500}) + (11.58 \pm 0.54), \quad (3)$$

and has a reduced-χ^2 of 1.60. For the N_{500} - T_x the best-fit relation is

$$Log(T_x) = (0.77 \pm 0.11) Log(N_{500}) + (-1.01 \pm 0.27), \quad (4)$$

and has a reduced-χ^2 of 2.46. The correlations have Root-Mean Squared (rms) scatters of 51% and 50% respectively. For the remainder of the paper, the percentage rms scatter in all correlations is computed using the same method as YE03. The rms deviation from the fit in terms of the dependent variable (in this case, M_{500}) is determined and then compared to its mean value from the entire sample.

The scatter in these correlations is larger than the 35% scatter in the local scaling relations measured by L04. However, the random errors in our data are larger than theirs, and clearly a portion of the scatter comes from these measurement errors. Given that the total scatter is the result of both the measurement errors in M_{500} and N_{500} as well as some intrinsic scatter, we estimate the intrinsic scatter by assuming that the measurement scatter is independent of the intrinsic scatter and then subtracting the mean measurement scatter of the dependent variable in quadrature from the total scatter. Using this simplistic method we estimate that the intrinsic scatter in N_{500} - M_{500} is 37% and for N_{500} - T_x it is 46%.

We compare the N_{500} values from the CNOC1 clusters with the L04 values in the top panel of Figure 3. L04 measured N_{500} by integrating the cluster LFs over an NFW spatial distribution and therefore it is the N_{500} within a spherical volume. Our N_{500} is measured using statistical background subtraction and is therefore the number of galaxies in a cylinder of radius R_{500}. We convert our N_{500} in cylinders to N_{500} in spheres by multiplying by a deprojection constant of 0.791, the value for the percentage difference in enclosed number of galaxies between spheres and cylinders at R_{500} for an NFW profile with c = 5. The dash-dot blue line in Figure 3 is the best-fit relation for the L04 clusters, and the solid red line is the best-fit relation for the CNOC1 clusters. The slope of the CNOC1 relations ($M_{500} \propto N_{500}^{0.71\pm0.11}$) is slightly shallower than the L04 relation that includes the BCGs ($M_{200} \propto N_{500}^{0.82\pm0.04}$), but is consistent within the errors. It is also consistent with the scaling relation found by Rines et al. (2004) for the CAIRNS clusters ($M_{200} \propto N_{200}^{0.70\pm0.09}$); however, their relation is measured using N_{200} and M_{200} and a different luminosity cut. The overall normalization of the CNOC1 N_{500} is nearly identical to the L04 normalization. As a comparison between the samples we plot the measured N_{500} values divided by those predicted from the local M_{500}-N_{500} relation in the bottom panel of Figure 3 . Figure 3 shows that the HON - mass correlation measured by L04 does not evolve between $z = 0$ and $z \sim 0.3$. The higher redshift CNOC1 clusters have N_{500} values which are only 4% ± 11% smaller than would be predicted by the local relation. The mean(median) $N_{500}/N_{500,fitlocal}$ is 0.96(0.90) ± 0.11, and is consistent with no evolution in the HON with redshift. As a comparison, the L04 clusters have a mean(median) $N_{500}/N_{500,fitlocal}$ of 1.04(1.01) ± 0.04.

The non-growth of the HON at a fixed mass with increasing redshift is different from the results of L04. In addition to their local clusters, L04 also computed the HON for a subset of clusters with $0.1 < z < 0.9$ (K-band imaging from De Propris et al. 1999) which had available X-ray temperatures and compared it to the local clusters. Their comparison showed that the HON was roughly a factor of 2 larger in the $z > 0.1$ clusters. From this they suggested that half of all cluster galaxies may be removed (via either merging or disruption) between $z \sim 0.6$ (all but two of their clusters are $z < 0.6$) and $z = 0$ in order to match the local HON.

It is unclear why the conclusions of our studies are so different. We did note in Paper I that it is challenging to reconcile the idea of a strong evolution of the cluster HON between $z \sim 0.6$ and $z = 0$ and the passive evolution of the K-band cluster LF. Paper I showed that the evolution of the cluster K^* tightly follows the prediction of a passive evolution model between $z \sim 0.5$ and $z = 0$ and those results reaffirmed the findings of the pioneering cluster K-band luminosity function study of de Propris et al. (1999), as well as recent K-band LFs of high-redshift clusters (e.g., Toft et al. 2003; Kodama & Bower 2003; Ellis & Jones 2002; Strazzullo et al. 2006). Interestingly, all of the $z > 0.1$ clusters used by L04 are part of the de Propris et al. (1999) sample. If 50% of cluster galaxies are either merged, or disrupted by tidal

forces between $z \sim 0.6$ and $z = 0$, then it seems unlikely that the evolution of K^* could follow a passive evolution model, unless the probability of being merged or tidally disrupted was independent of galaxy K-band luminosity (i.e., stellar mass). While mass-independence may be plausible in the case of mergers, more massive galaxies are more difficult to disrupt. If a significant number of disruptions do occur, they should preferentially destroy galaxies on the faint-end of the luminosity function and therefore will change its overall shape.

L04 appeal to the N-body simulations of Kravtsov et al. (2004) for an explanation of the strong redshift evolution of the HON. Kravtsov et al. (2004) show that for dark matter halos, the HON at a given mass becomes approximately a factor of three larger from $z = 0$ to $z = 5$. They show that the dark matter HON at a given mass is smaller at lower redshift because low mass halos merge with high mass halos as well as become tidally truncated or disrupted by massive halos in high-density regions such as clusters.

More recent simulations which incorporate both dark matter as well as baryonic matter using Smoothed Particle Hydrodynamics (SPH, e.g., Nagai & Kravtsov 2005, Weinberg et al. 2006) show that when the baryonic component is included, the interpretation of the HON derived by counting galaxies becomes more subtle. Nagai & Kravtsov (2005) simulated a set of 8 clusters and found that as subhalos enter the cluster R_{200} they are stripped of ∼30% of their total dark matter mass. Once they fall into the cluster they are further stripped until ∼70% of their original dark matter mass is removed. Their result confirms the earlier N-body simulations which showed the dark matter HON is depleted with decreasing redshift, especially in high-density environments; however, the SPH simulations also show that primarily the dark matter is stripped from the halos and very little of the baryonic mass (in the form of stars and gas) is lost during this process. The baryonic matter remains because it tends to cool, and fall to the center of the subhalo and is amongst the most tightly bound mass in the subhalo.

These simulations suggest that the HON, when selected by counting the number of massive dark matter subhalos is quickly depleted in high density regions such as clusters because of tidal stripping and merging of the subhalos. However, when the HON is selected by the baryonic mass of halos (i.e., using K-band number counts) there should be little evolution in the HON at a given halo mass, because the baryonic component of subhalos is tightly bound, and will only be depleted in the case of full disruption. This interpretation is consistent with our data and is also consistent with the observation that both K^* (Paper I, L04, de Propris et al. 1999) and α (L04) for cluster galaxies are basically identical across more than an order-of magnitude in cluster mass (Paper I, L04, de Propris et al. 1999). Given that the efficiency of tidal stripping is correlated with cluster mass, it is hard to understand how the K-band LF of cluster galaxies could be independent of cluster mass unless the baryonic component is unaffected in the process.

In summary, we find that the K-band selected HON of clusters at a given mass does not evolve significantly between $z = 0$ and $z \sim 0.3$. This result is consistent with the more recent work of Lin et al. (2006) who measured the HON within R_{2000}, R_{1000} and R_{700} for a sample of 27 clusters $0 < z < 0.9$ (a few of which are included in L04) and also find no-evolution in the HON at fixed mass. We argue that the non-evolution of the HON is naturally explained by recent SPH simulations, which show that while dark matter halos encounter a significant amount of tidal stripping in high-density regions such as clusters, the baryonic component within remains mostly intact. Furthermore, this interpretation reconciles the strong tidal stripping with the purely passive evolution of the cluster K-band LF, and its invariance across the cluster mass spectrum.

Our data cannot rule out the possibility that the simulations may over-exaggerate the tidal stripping and that similar to the baryonic component, the dark matter mass-selected HON at a fixed cluster mass also does not evolve within the same redshift range. A useful way to test this would be to compare the M/L ratios of cluster galaxies and field galaxies at large radii and look for evidence of truncated halos within the cluster population. Unfortunately, this is a challenging task, because there are few tracers of the dark matter potential at large radii for galaxies. There is now evidence from galaxy-galaxy lensing studies of massive clusters that supports the tidal-stripping scenario (Halkola et al. 2006, Natarajan et al. 2002); however, in lower-mass clusters ($M \sim 10^{13}$-10^{14} $M_\odot$), the same trend is not observed (Mandelbaum et al. 2006). A more comprehensive study of galaxy-galaxy lensing in clusters in the range of $M \sim 10^{14}$-10^{15} $M_\odot$ would be particularly useful for testing this interpretation.

5. K-BAND LIGHT AND RICHNESS AS AN INDICATOR OF CLUSTER MASS

In this section we measure the total K-band luminosity within R_{200} for the clusters ($L_{200,K}$) and examine its correlation with cluster mass. We also determine the correlation between K-band selected richness and cluster mass.

5.1. *Total K-Band Luminosity*

$L_{200,K}$ for a galaxy cluster is defined as the sum of the K-band luminosity of all cluster galaxies within R_{200} to a fixed absolute magnitude. In principle the measurement is straightforward; however, in practice, data are never homogeneous and additional corrections must be applied. In the case of the CNOC1 clusters, the clusters lie at a fairly large range of redshifts and therefore the light from each galaxy must be both k-corrected and evolution corrected to a common redshift. The need for these corrections means that the membership and approximate spectral-type for each galaxy in the cluster field must be determined. This is not as precise using statistical background subtraction and therefore we make use of the extensive spectroscopic catalogues. The spectroscopy is complete to $K^* + 1$ for all clusters, but is sparsely sampled. Therefore, a spectroscopic selection function is used to correct for the sampling. The method for determining the spectroscopic selection function was developed by the CNOC1 (Yee et al. 1996) & CNOC2 (Yee et al. 2000) collaborations and is discussed in detail in those papers as well as Paper I. Similar to the analysis in Paper I, we ignore the "secondary" selection effects (color, position, and z) and use only the magnitude weights, which are the overwhelmingly dominant

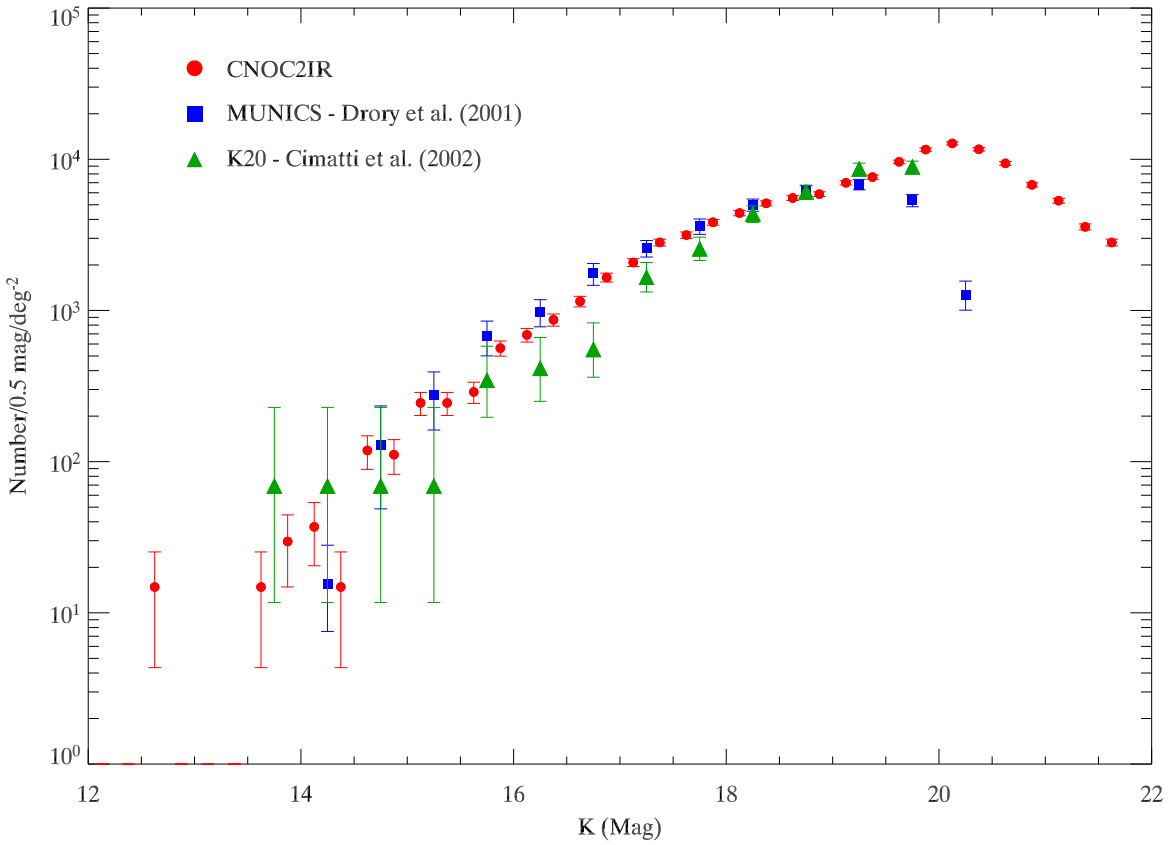

FIG. 1.— *Red Dots*: Number of galaxies per square degree per 0.5 magnitudes as a function of magnitude determined from 0.26 square degrees of CNOC2 K-band imaging data. *Green Triangles*: Number counts from the K20 Survey. *Blue Squares*: Number counts from the MUNICS Survey.

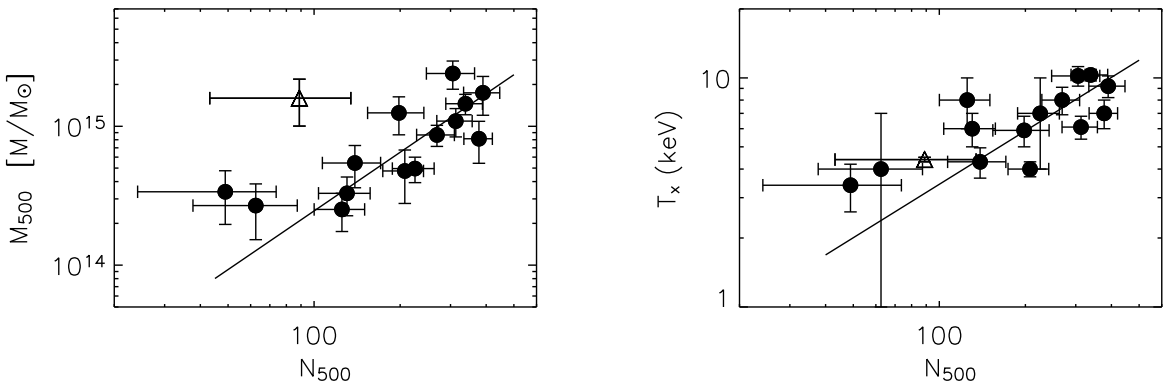

FIG. 2.— Left Panel: Plot of M_{500} vs. N_{500} for the CNOC1 clusters. The solid line is the best-fit linear relation and has an rms scatter of 50%. Right Panel: Plot of T_x vs. N_{500} for the same clusters. The solid line is the best-fit linear relation and has an rms scatter of 51%. MS1455+22 is plotted as an open triangle.

selection bias (Yee et al. 1996).

The k-correction for each galaxy is taken from the models of Poggianti (1997). The k-corrections depend only mildly on spectral-type and the color/spectral-type model discussed in Paper I is used to estimate a spectral-type for each galaxy. Also, the LFs from Paper I showed that the luminosity evolution in the clusters is passive, but significant (0.35 ± 0.06 magnitudes from $z = 0$ to $z \sim 0.5$). Therefore, an evolution correction from the Poggianti (1997) models is applied to each galaxy, where we have transformed the Poggianti (1997) evolution corrections to our cosmology (see Paper I, §6.1.2). By applying both k and evolutionary corrections the measured $L_{200,K}$ is corrected to $z = 0$, and therefore these values can be directly compared to local studies.

The $L_{200,K}$ for some clusters must also be corrected for the incomplete coverage of R_{200}. We noted that for the HON (§4) the coverage corrections propagate to large errors in the HON when it is computed within R_{200} and because of that, the HON was measured within R_{500}. The incomplete radial coverage is less problematic when computing $L_{200,K}$ because much of the total cluster luminosity comes from the BCG ($\sim$ 5 - 30%). Despite the fact that the number of cluster galaxies at $R_{500} < R < R_{200}$ is large, the most luminous galaxies tend to reside in the cluster core, and therefore galaxies at $R_{500} < R < R_{200}$ contribute less to the total luminosity than to the HON.

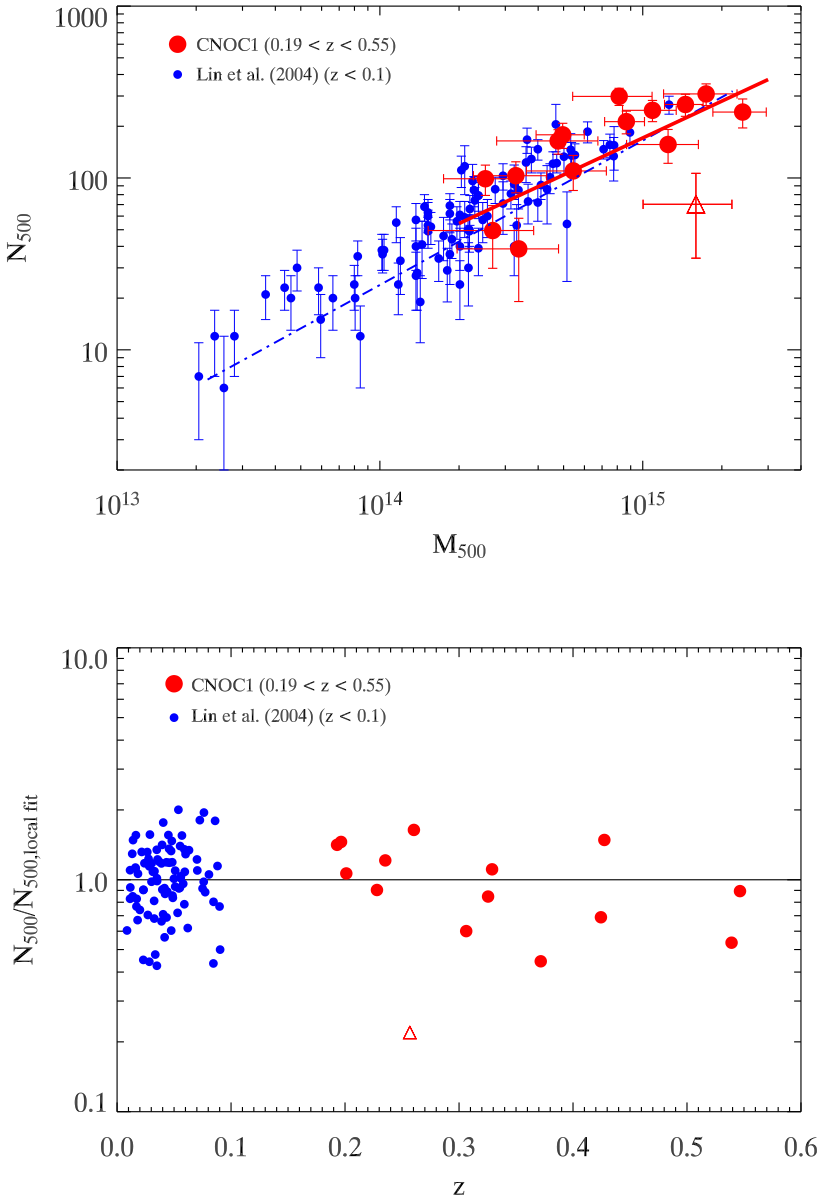

FIG. 3.— *Top Panel*: Plot of N_{500} vs. M_{500} for the CNOC1 clusters (large red points) and the L04 clusters (small blue points). MS1455+22 is plotted as an open triangle. The solid red line is the best-fit relation for the CNOC1 clusters, and the dash-dot blue line is the best-fit relation for the L04 clusters. The slope is the CNOC1 correlation is slightly shallower, but consistent with the L04 slope. *Bottom Panel*: Plot of the measured N_{500} divided by the value predicted by the L04 scaling relation as a function of redshift for the L04 clusters (blue points) and CNOC1 clusters (red points). The CNOC1 normalization is consistent with the L04 normalization suggesting no evolution in the HON with redshift.

The clusters without complete coverage have been observed in a strip through the cluster core; therefore, the coverage problems are corrected by computing the luminosity in circular shells. The total luminosity of a shell is multiplied by the ratio of the total area of the shell, to the total area of the shell with imaging/spectroscopic data. Several of the clusters (MS0016+16, MS0451-02, MS1006+12, MS1008-12, and MS1455+22) have no coverage for a few of the outermost shells. For these clusters a correction based on the profile of clusters which have the best coverage in the outer regions is applied. This correction is small in four of the five cases ($\sim$ 5-10%), again because the majority of the cluster light comes from the core. MS1455+22 has a very large R_{200} (which is likely to be overestimated, see §4) and therefore the correction is much larger ($\sim$ 60%).

Once the selection function, k-correction and evolution corrections have been applied, and the sum of the luminosity of galaxies brighter than K* + 1 has been tabulated, the "total" luminosity of the cluster is finalized by extrapolating the LF to a fixed absolute magnitude. We choose to extrapolate to M_K = -21 (i.e., K* + 3 at z = 0), the same limiting absolute magnitude used by L04 and and effectively the same limiting magnitude of the HON. We evolution-correct the combined LF from all 15 clusters to z = 0 (K* = -24.14 $\pm$ 0.15 and α = -0.84 $\pm$

0.08, see Paper I) and use this for extrapolation. This LF is consistent with the average LF found by L04 (K^* = -24.02 ± 0.02 and α = -0.84 ± 0.02) and because our clusters have been evolution corrected to $z = 0$, extrapolating the luminosity to M_K = -21 results in a $L_{200,K}$ which can be directly compared between the samples. Before the correction is applied, the contribution from the BCGs is removed from the total cluster light. The BCGs contribute a significant, but variable, fraction of the total cluster light ($\sim$ 5-30% at $K^* + 1$) and do not obey a Schechter function. Including them as part of the extrapolation of the Schechter function would overestimate the total cluster light. The light from the BCG galaxy is re-added to the total once the extrapolation has been done. Lastly, a bootstrap error for each cluster is computed by performing the entire analysis using 300 resamplings with replacement from the data. Table 2 lists the final $L_{200,K}$ values as well as the bootstrap errors.

We examine the correlation between the cluster mass and light by plotting Log(M_{200}) vs. Log($L_{200,K}$) in the first panel of Figure 4. The best-fit linear relation is

$$Log(M_{200}) = (1.20 \pm 0.16) Log(L_{200,K}) - (0.95 \pm 2.21), \quad (5)$$

and the fit has a reduced-χ^2 of 2.65, where again we have ignored MS1455+22 because it is likely to have an incorrect M_{200}. The rms scatter in the M_{200} - $L_{200,K}$ relation is 43% and from this we estimate that the intrinsic scatter is 31%. The scatter in the correlation is about a factor of 1.3 larger than the 34% total, and 24% intrinsic scatter measured by L04 for local clusters. If we invert the axes, we find $L_{200,K} \propto M_{200}^{0.83\pm0.11}$. This agrees with the scaling relation for local clusters with the BCG included which is $L_{200,K} \propto M_{200}^{0.72\pm0.04}$ (L04), and somewhat less well with the scaling relation for local groups which is $L_{200,K} \propto M_{200}^{0.64\pm0.06}$ (Ramella et al. 2004). This shows that the slope, while slightly shallower for groups, does not change significantly over $\sim$ 2 orders of magnitude in cluster mass. Furthermore, the reasonable agreement between the slope and intrinsic scatter in the correlations at different redshifts suggests that whatever physical processes are responsible for building in the correlation have largely taken place by $z \sim 0.3$, and that there is little change in the L_{200} - M_{200} relation from $z \sim 0.3$ to $z = 0$, besides possibly a small decrease in the scatter.

In the second panel of Figure 4 we plot the correlation between the cluster X-ray temperature and $L_{200,K}$. The best fit relation with MS1455+22 excluded is

$$Log(T_x) = (0.77 \pm 0.08) Log(L_{200,K}) + (-9.45 \pm 1.07), \quad (6)$$

and has a reduced-χ^2 of 2.35. The rms scatter in the relation is 24% and this corresponds to an intrinsic scatter of 14%, notably better than the M_{200} - $L_{200,K}$ relation. As the CNOC1 clusters are all massive, relaxed X-ray systems, this may not be surprising. Using r-band data, YE03 found the correlation between B_{gc} and T_x for the CNOC1 clusters to have a smaller scatter (21%) than the B_{gc} - M_{200} relation (31%), although they used the T_x values determined by Lewis et al. (1999) rather than the Hicks et al. (2006) values.

If we compare the scatter in the M_{200} vs. $L_{200,K}$ relation to the scatter in the correlations of M_{200} vs. T_x, L_x, and B_{gc} (optical) determined by YE03 for these clusters, we find that the total K-band light is approximately as accurate as those parameters in inferring the dynamical mass. YE03 showed the scatter in the M_{200} vs. T_x, L_x, and B_{gc} (optical) for these clusters was 29%, 35%, and 31% respectively. This demonstrates that $L_{200,K}$ is as good as, but no more accurate than traditional mass indicators at inferring the cluster dynamical mass. It appears the fact that K-band light is a fairly clean tracer of an individual galaxy's stellar mass does not result in a smaller scatter for the $L_{200,K}$ - M_{200} scaling relation, suggesting that the amount of scatter measured in optical scaling relations is a real scatter in relative amounts of stellar mass and dark matter mass in clusters, and not enhanced due to a variance in star-formation properties or stellar populations from cluster-to-cluster.

It is possible that the scatter we measure is enhanced by systematics in the data analysis caused by the need for k-corrections, evolution corrections, spectroscopic selection functions, and coverage corrections; however, the level of scatter we find is of order that found by L04 in local clusters, which do not suffer from those uncertainties. Given that there is no reason to expect the scatter in the scaling relations to become *smaller* at higher-redshift, it would suggest that these corrections have been applied properly and do not significantly increase the overall scatter.

The correlations from Figure 4 are pleasing in the sense that total K-band light is observationally much cheaper to measure than L_x, T_x or M_{200} (via a velocity dispersion or weak lensing) for a given cluster. For clusters in this redshift range, a wide-field NIR camera on a 4m-class telescope can achieve a limiting magnitude of $M_K < K^* + 1$ with an integration time of only a few minutes. This means followup of many candidates in the generation of high-yield cluster cosmology projects is easily achievable. Unfortunately, a major concern for cosmology projects is that although $L_{200,K}$ appears to be a good proxy for M_{200} or T_x it cannot be used in practice because it requires an *a priori* knowledge of R_{200}. In the next section we show that the NIR-selected richness in a fixed aperture is also well-correlated with the cluster mass and can be used as a mass proxy.

5.2. *B_{gc} as an Indicator of Cluster Mass*

The good correlation between $L_{200,K}$ and M_{200} found for the CNOC1 clusters, and by other authors (e.g. Lin et al. 2003; L04; Rines et al. 2004; Ramella et al. 2004) demonstrates that K-band light can be used as an efficient estimator of the cluster halo mass. Of course, measuring $L_{200,K}$ requires knowledge of R_{200}, which is generally an unknown, whereas the cluster richness, parameterized by B_{gc} does not require R_{200}. B_{gc} is the amplitude of the 3-dimensional, spatial correlation function between the cluster center and the cluster galaxies. If the shape of the 2-dimensional angular correlation function is assumed (i.e., $w(\theta) \propto \theta^{(1-\gamma)}$, with $\gamma \sim 1.8$), then its amplitude can be measured by counting galaxies in a fixed aperture around the cluster center. B_{gc} is then measured by deprojecting the angular correlation function via ($\xi(r) \propto r^{-\gamma}$) and scaling it by a luminosity function. A full derivation and motivation for B_{gc} is presented in Longair & Seldner (1979). The B_{gc} parameter

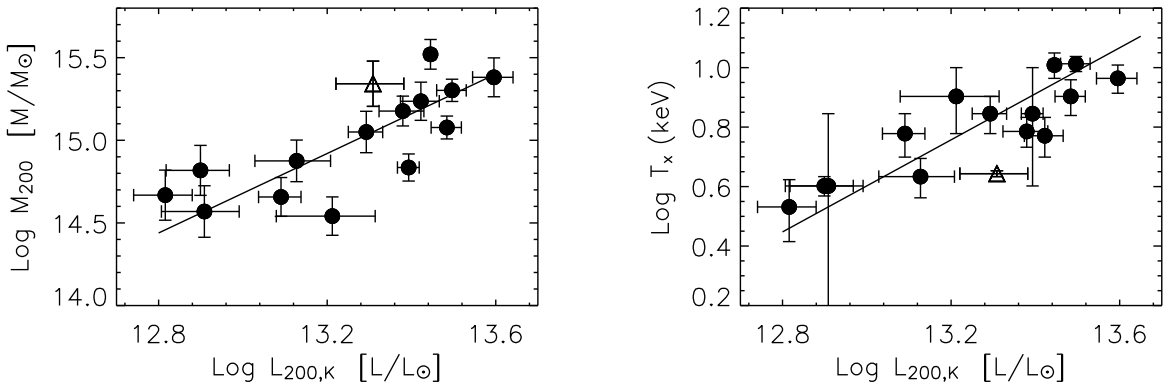

FIG. 4.— Left Panel: Plot of Log(M_{200}) vs. Log($L_{200,K}$) for the CNOC1 clusters. The solid line is the best-fit linear relation. The rms scatter around the relation is 43% (31% intrinsic). Right Panel: Plot of T_x vs. Log($L_{200,K}$). The solid line is the best-fit linear relation and as an rms scatter of 24% (14% intrinsic). MS1455+22 is plotted as an open triangle in both panels and is excluded in the fits.

is defined as:

$$B_{gc} = \mathrm{N}_{net}\frac{(3-\gamma)\mathrm{D}^{\gamma-3}\theta^{\gamma-1}}{2\mathrm{A}_\theta \mathrm{I}_\gamma \Psi[\mathrm{M}(\mathrm{m}_0,z)]}, \quad (7)$$

where N_{net} is the background corrected cluster galaxy counts, D is the angular diameter distance to the cluster redshift, θ is the angular size of the counting aperture, A_θ is the angular area of the counting aperture, I_γ is geometric deprojection constant which depends on γ (I_γ = 3.78 for $\gamma \sim 1.8$), and Ψ is the integrated cluster LF up to the apparent magnitude M, which corresponds to an absolute magnitude m_0 at the redshift z. The normalization of the LF (ϕ^*) is the universal normalization, and not the cluster normalization, so that B_{gc} is the overdensity of galaxies compared to the field density, not the average cluster density. This formula for B_{gc} is slightly different than formula presented in Yee & Lopez-Cruz (1999, their equation 3) in that it contains the A_θ term. We note that in their formula for B_{gc}, Yee & Lopez-Cruz (1999) had inadvertently left out the A_θ term due to a transcribing error.

At first, B_{gc} may appear to be an unnecessarily complicated measure of the cluster richness; however, using it has some distinct advantages. As interest in an observationally cheap proxy for cluster mass has increased, so have the number of studies which have looked at the correlation between cluster richness and mass (e.g., Hansen et al. 2005; Miller et al. 2005; Gilbank et al. 2004; L04; Rines et al. 2004; Ramella et al. 2004; Lin et al. 2003; Kochanek et al. 2003; YE03). These studies define the cluster richness as the number of galaxies within a fixed aperture, to a fixed magnitude limit. However, because different authors use different apertures, and different magnitude limits, comparison between studies is extremely difficult. The advantage of the B_{gc} parameter is that it assumes a universal spatial distribution, and luminosity function for clusters. Therefore, aside from statistical fluctuations, *the value of B_{gc} is, in principle, identical regardless of what aperture is used to count galaxies, and which magnitude limit is chosen.*

Yee & Lopez-Cruz (1999) verified this was true, but showed that measuring B_{gc} from a fixed aperture with R = 500 kpc (using H_0 = 50 km s^{-1} Mpc^{-1}) produced the lowest statistical errors. Furthermore, they showed that counting galaxies to $M < M_* + 1$ was all that was required for B_{gc} to be robust. Therefore, our values of $B_{gc,K}$ are computed using a fixed aperture of 500 kpc (although we use H_0 = 70 km s^{-1} Mpc^{-1}) and by counting galaxies to $K^* + 1$.

Again, because B_{gc} requires counting the number of cluster members, we use statistical background subtraction, rather than the spectroscopic weights. YE03 demonstrated that B_{gc}'s computed using both techniques agree extremely well. In order to determine the integrated LF parameter ($\Psi[M(m_0,z)]$) a universal cluster luminosity function must be assumed. We showed in Paper I that besides the passive evolution of the stellar populations, this is a reasonable assumption for the CNOC1 clusters. When calculating $\Psi[M(m_0,z)]$ we assume passive evolution of the LF of our "average" cluster (K^* = -24.14, α = -0.84). Unfortunately, we do not have a measurement of the universal ϕ^* in units of Number/Mpc^3. This cannot be determined from the cluster data alone because clusters are high-density regions in the universe, and not representative of the mean value of ϕ^*. Rather than using values from studies of the K-band field LF (which still have fairly large errors) we adopt the approach of Yee & Lopez-Cruz (1999) for determining ϕ^*. They showed that a self-consistent value of ϕ^* could be estimated by evolving the cluster LF assuming a simple model for the evolution of $M^*(z)$. The normalization (ϕ^*) is determined by requiring that the integrated counts from the LF reproduce the background galaxy counts. We perform the same procedure using a $z_f = 5.0$ model passive evolution model (see Paper I) to parameterize the evolution of $M^*(z)$. By comparing the model background counts to the true background counts and using a χ^2-maximum-likelihood technique we determine $\phi^* = 4.34 \times 10^{-3}$ Mpc^{-3}. This value of ϕ^* is slightly larger than the $\phi^* = 3.40 \pm 0.29 \times 10^{-3}$ Mpc^{-3} determined locally (Kochanek et al. 2001), and about 3 times as large as the $\phi^* = 1.78^{+1.5}_{-0.9} \times 10^{-3}$ Mpc^{-3} measured at $0.2 < z < 0.65$ by Pozzetti et al. (2003). However, even if this value is incorrect it will be systematically incorrect for all clusters and will only affect the intercept in the correlation between $B_{gc,K}$ and other physical parameters. It will not affect the slope or scatter, which are of principle interest.

Column 6 of Table 2 lists the measured values of B_{gc} for the clusters. The errors have been computed using the prescription from Yee & Lopez-Cruz (1999),

$$\frac{\Delta B_{gc,K}}{B_{gc,K}} = \frac{(N_{net} + 1.3^2 N_{bg})^{1/2}}{N_{net}}, \quad (8)$$

where N_{bg} is the number of background counts within the 500 kpc and the 1.3^2 term is used to approximately account for the clustering of background galaxies.

In the left panel of Figure 5 we plot $\mathrm{Log}(B_{gc,K})$ vs. $\mathrm{Log}(M_{200})$ for the clusters. The best fit linear relation with MS1455+22 excluded is

$$Log(M_{200}) = (1.62 \pm 0.24) Log(B_{gc,K}) + (9.86 \pm 0.77). \quad (9)$$

The fit has a reduced-χ^2 of 1.29, and the rms scatter of the correlation is 35% (18% intrinsic). This implies that the K-band selected richness is slightly better than the total K-band light for predicting the mass of a galaxy cluster. The difference in total and (intrinsic) scatter between the two parameters is notable, 35%(18%) in M_{200} - $B_{gc,K}$ vs. 43%(31%) in M_{200} - $L_{200,K}$ and this may be because of the smaller aperture used to measure B_{gc}.

In the right panel of Figure 5 we plot $\mathrm{Log}(B_{gc,K})$ vs. $\mathrm{Log}(T_x)$. The best fit linear relation with MS1455+22 excluded is

$$Log(T_x) = (0.94 \pm 0.13) Log(B_{gc,K}) - (2.20 \pm 0.42), \quad (10)$$

and has a reduced-χ^2 of 2.00 and an rms scatter of 25% (16% intrinsic). This is very similar to the scatter seen in the $L_{200,K}$ - T_x relation and shows that the fixed-aperture richness is an excellent indicator of the cluster X-ray temperature at the $\sim 25\%$ level.

If we compare the accuracy of $B_{gc,K}$ to the optical B_{gc} we find that they are almost identical at predicting M_{200} (scatters of 35%, and 31% respectively) as well as T_x (scatters of 25% and 21% respectively). $B_{gc,K}$ for the CNOC1 clusters also has a similar scatter to the fixed-aperture richnesses measured for local clusters in the K-band. L04 showed that the scatter in the number of galaxies within 0.75 Mpc vs. M_{500} was 43%, and estimated that $\sim 24\%$ of the scatter was intrinsic. The L04 cluster masses are measured using T_x and therefore the it is more relevant to compare the L04 intrinsic scatter to the intrinsic scatter in the CNOC1 B_{gc} - T_x relation. The scatter in the L04 relation is somewhat larger than the scatter from the CNOC1 relation, but this may be due to the fact that the CNOC1 clusters are generally more massive than the L04 clusters.

These results demonstrate that relatively cheap IR imaging can be used to determine cluster masses with good accuracy. Specifically, IR imaging of even higher redshift clusters ($z > 0.5$) will be valuable for determining masses in large optical cluster surveys. IR richnesses will likely be more robust than optical richnesses at predicting cluster masses at high-redshift because at high-redshift optical bandpassess probe bluer parts of a galaxy's spectrum where the star-formation properties can drastically alter a galaxy's luminosity.

It is also possible that in the case of large cluster surveys, $B_{gc,K}$ may prove to be as valuable for predicting the cluster halo mass as the cluster velocity dispersion or X-ray temperature. Determining the cluster mass from either the line-of-sight velocity dispersion or X-ray temperature require assumptions about the dynamical state of the cluster. Dynamical masses require that the cluster is in virial equilibrium and that that the shape of the velocity ellipsoid is known (generally it is assumed to be isotropic). X-ray masses require the assumption of hydrostatic equilibrium, and spherical symmetry. They also require a correction if the cluster has a cooling flow. In cases where these assumptions do not apply (such as cluster-cluster mergers, or a collapsing system in the process of forming) the masses of the clusters may be poorly estimated, and these clusters will contaminate the measurement of the cluster mass function. The number of catastrophic outliers can have serious consequences on the measured cosmological parameters because they are particularly sensitive to the number of rare, massive clusters. On the other hand, if clusters which are unrelaxed, or currently undergoing a merger do not have the K-band light of their galaxies altered significantly, then using K-band richness as a mass indicator could potentially be a robust method for determining the masses of clusters that are not in dynamical or hydrostatic equilibrium.

One way to test this hypothesis is to use weak-lensing to measure the mass of clusters and compare those masses to B_{gc}, and $B_{gc,K}$. Weak-lensing does not require any assumptions about the dynamical state of the clusters and therefore it is an unbiased (although statistically noisy) measure of the cluster mass. Weak lensing masses for a subsample of the CNOC1 clusters have been measured and will be compared to $B_{gc,K}$ in a future paper.

6. THE K BAND MASS-TO-LIGHT RATIO

Recent studies of the K-band M/L ratio in local clusters (Lin et al. 2003, L04, Rines et al. 2004, Ramalla et al. 2004) have shown that the K-band cluster M/L ratio is an increasing function of cluster mass (although Kochanek et al. 2003 find it is roughly constant with mass). These studies have also found that the M/L ratio is a slowly decreasing function of radius, with the integrated M/L ratio at R_{200} ($M_{200}/L_{200,K}$) being $\sim 15\%$ smaller than the M/L ratio at R_{500} (e.g., L04). Here we present the first K-band M/L ratios of massive, intermediate-redshift clusters.

We use the k and evolution corrected $L_{200,K}$ values to compute $M_{200}/L_{200,K}$ and therefore it is the $M_{200}/L_{200,K}$ ratio of clusters corrected to $z = 0$. The values are listed in Table 3 and the errors computed by propagating the M_{200} and L_{200} errors in quadrature. In Figure 6 we plot $\mathrm{Log}(M_{200}/L_{200,K})$ vs $\mathrm{Log}(M_{200})$. There is a clear correlation of M/L with M_{200} in the CNOC1 clusters. The Spearman rank-correlation coefficient for these data is 0.60, which implies a probability of 0.017 that the variables are uncorrelated. The solid line in the plot is the best-fit linear relation with MS1455+22 excluded:

$$Log(M_{200}/L_{200,K}) = (0.57 \pm 0.13) Log(M_{200}) - (6.92 \pm 2.04). \quad (11)$$

The fit has a reduced-χ^2 of 0.964 and implies that M/L $\propto M^{0.57\pm0.13}$. Interestingly, this slope is about a factor of 3 steeper than the M/L $\propto M^{0.17\pm0.11}$ that would be inferred using the $\mathrm{Log}(M_{200})$ - $\mathrm{Log}(L_{200,K})$ relation (Eqn 5) where the variables are less directly correlated (they still both depend on R_{200}). As a comparison, the inferred relation is plotted as the dashed line in Figure 6. The inferred relation, M/L $\propto M^{0.17\pm0.11}$, agrees well with the relation from local clusters where M/L $\propto M^{\alpha}$ with $\alpha = 0.26 \pm 0.04$ (L04), and $\alpha = 0.31 \pm 0.09$ (Rines et al. 2004), but does not agree well with the value for local groups, $\alpha = 0.56 \pm 0.05$ (Ramella et al. 2004). The Ramella et al. relation is similar to the correlation obtained by fitting Log(M/L) vs. $\mathrm{Log}(M_{200})$ directly.

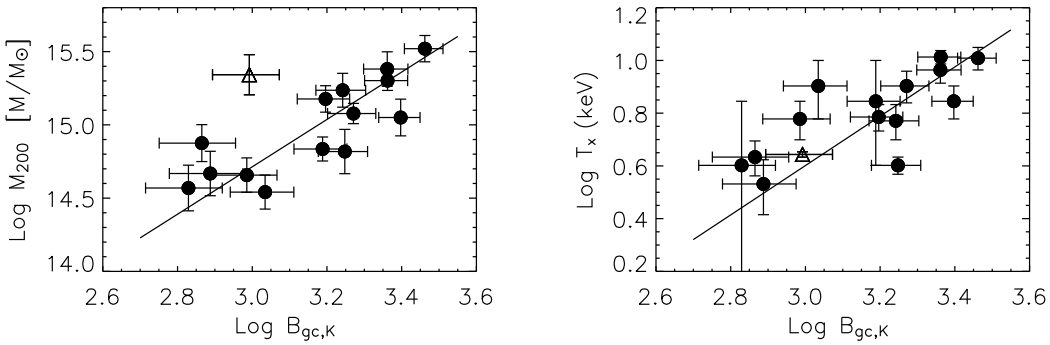

FIG. 5.— Left Panel: Plot of Log(M_{200}) vs. Log($B_{gc,K}$) for the CNOC1 clusters. The solid line is the best-fit linear relation and has an rms scatter of 35% (18% intrinsic). Right Panel: Plot of Log(T_x) vs. Log($B_{gc,K}$) for the same clusters. The solid line is the best-fit linear relation and has an rms scatter of 25% (16% intrinsic). MS1455+22 is plotted as an open triangle in both panels and is excluded in the fits.

It is likely that the inconsistent slopes from our own data, as well as between the local cluster and group M/L vs. M_{200} are primarily caused by the large scatter in the M_{200} - $L_{200,K}$ scaling relations and the difficulties associated in fitting to data with a larger scatter than is accounted for by the error bars. It is probably not caused by real differences in the M/L vs. M_{200} scaling relations for the different cluster samples. In our own data the M_{200} - $L_{200,K}$ relation has a large reduced-χ^2 (2.65). Examination of Figure 4 suggests that the inflated reduced-χ^2 is not caused by a linear fit being the incorrect model for these data, but is caused by a handful of significant outliers to the relation.

Another consideration is that the intrinsic correlation between M/L and M_{200} (mass is in both parameters) can contribute to the discrepancy in slope. The Ramella et al. (2004) masses and our own masses are determined from the cluster velocity dispersion (σ_1) and equation 2, where $M_{200} \propto \sigma_1^3$. The L04 masses are determined from T_x using the fit from Finoguenov et al. (2001) where $M_{200} \propto T_x^{1.58}$. Given that M_{200} depends on σ_1^3 but only on $T_x^{1.58}$, catastrophic errors in σ_1 will translate to larger errors in M_{200} than catastrophic errors in T_x will. Consequently, given that the Log(M/L) vs. Log(M_{200}) slope is < 1, clusters which have their velocity dispersions incorrectly measured (and not properly accounted for by the errors, such as in the case of non-virialization) will steepen the slope of the M/L vs. M_{200} correlation because the mass term is in both parameters.

As a test, we remove the highest and lowest mass CNOC1 clusters (MS0440+02 and MS0451-03, both of which are significant outliers in the M_{200} - L_{200} relation) and refit. We find a slope of $\alpha = 0.44 \pm 0.15$, which is more consistent with the $\alpha = 0.17 \pm 0.11$ inferred directly from the M_{200} vs. $L_{200,K}$ relation. Unfortunately, this problem of outliers makes determining a robust slope for the M/L vs. M_{200} correlation difficult. The data are less directly correlated in the case of Log(M_{200}) vs. Log($L_{200,K}$), and therefore we return to that relation and adopt $M_{200}/L_{200,K} \propto M^{0.17\pm0.11}$ as the best slope for M/L vs. M_{200} scaling relation for the CNOC1 clusters.

This slope, where M/L increases with increasing M_{200} supports the scenario proposed by both L04 and Rines et al. (2004), where either the star-formation efficiency of cluster galaxies is a decreasing function of cluster mass, or else that the amount of intra-cluster light is an increasing function of cluster mass. Interestingly, the slope of this scaling relation for the CNOC1 clusters is consistent with the the slope in local clusters and this shows that the M/L vs. M_{200} correlation is in place by at least $z \sim 0.3$, roughly 4 Gyr in lookback time.

7. Ω_M FROM THE OORT TECHNIQUE

The original purpose of the CNOC1 project was to measure the cosmological density parameter $\Omega_{m,0} \equiv \rho_o/\rho_c$ using the Oort (1958) technique. The cluster M/L ratio, divided by the M/L ratio for closure $(M/L)_c \equiv \rho_c/j$, where j is the field luminosity density, provides a direct measure of $\Omega_{m,0}$ which is independent of the Hubble parameter. There has been some concern with this method because recent numerical simulations suggest that light is a biased tracer of dark matter, and that the M/L ratio of any region in the universe which contains galaxies automatically provides an underestimate of the universal M/L ratio, and an underestimate of $\Omega_{m,0}$ (e.g., Ostriker et al. 2003). However, this is only a significant concern for low-density regions in the universe (i.e., the group scale or less). Unlike those lower density regions, rich clusters are assembled from regions of > 10 Mpc across (Carlberg et al. 1997) and therefore, provided that observations extend to the entire volume of the cluster (i.e., $R \sim R_{200}$), clusters should contain a sufficient collapsed volume to provide a representative sample of the universal M/L ratio (e.g. Carlberg et al. 1996, Carlberg et al. 1997). This is yet to be verified in numerical simulations as, until recently, they lacked enough volume to contain rich clusters. The CNOC1 project was designed specifically with this biasing concern in mind and therefore is a wide-field study of a sample of rich clusters.

Although biasing is not a major concern for the cluster technique, we know that the stellar populations of galaxies in the cluster and field environments are different (e.g., Ellingson et al. 2001, Balogh et al. 1999, Poggianti et al. 1999, Dressler et al. 1997) and without a good understanding on how these differences affect the integrated luminosity of these regions, there arises the potential for a systematic error in $\Omega_{m,0}$.

Using the r-band data for the CNOC1 clusters, Carlberg et al. (1997) showed that $\Omega_{m,0} = 0.19 \pm 0.06$ (random) $\pm$ 0.04 (systematic). In their analysis they found that the r-band cluster galaxies were on average 0.11 ± 0.05 mag fainter than field galaxies at this redshift and hence they decreased the cluster M/L ratio accordingly. Given the need for this correction, it is advantageous to perform the same analysis with infrared data, because

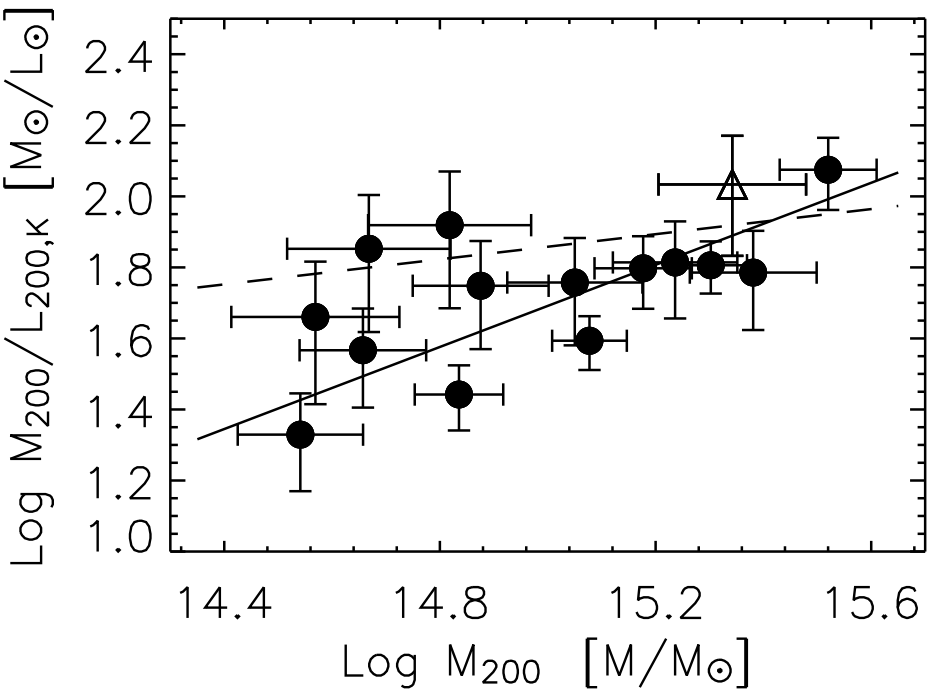

FIG. 6.— Plot of Log($M_{200}/L_{200,K}$) vs Log(M_{200}) for the CNOC1 clusters. The solid line is the best-fit relation. The dashed line is the relation that is inferred from the Log(M_{200}) - Log($L_{200,K}$) fit. MS1455+22 is plotted as an open triangle and is excluded in the fit.

infrared light is a better tracer of total stellar mass than optical light. The infrared luminosity of galaxies does not depend strongly on the current star-formation properties of the stellar population and consequently, little or no correction is required to account for the varying star-formation properties of the field and cluster environment. The only potential correction required would be if the cluster environment played a role in the star-formation *efficiency* of galaxies. A differing star-formation efficiency could manifest itself in two ways: 1) the stellar mass may be distributed differently in the cluster/field environment (i.e., the *shape* of the field and cluster LFs may be different); or 2) baryons may be converted into stars at a different rate than in the field (i.e., the ratio of the stellar mass to dark matter mass could be different between these environments).

In terms of problem 1), Paper I showed that the cluster K^* was brighter than, but consistent with the field value ($\Delta K^* = 0.25 \pm 0.26$ mag). Paper I also showed that α from the CNOC1 cluster LF was the same as α for local clusters as well as the local field. Those results agreed well with local measurements which showed the cluster K^* and α are roughly the same as the field (although we note that both L04 and Rines et al. 2004 find that the cluster K^* is ~ 0.2 mag brighter at the 2σ level). Given that both K^* and α for the cluster LF are similar to the field LF, the distribution of galaxies in terms of luminosity (and by corollary stellar mass) should be similar in both environments.

In terms of problem 2), it is important to note that the cluster M/L ratio continues to be an increasing function of cluster mass, even for objects as massive as the CNOC1 clusters. This shows that the overall rate of converting baryons to stars is a function of environment. The rich CNOC1 clusters have a K-band M/L ratio which is about an order of magnitude larger than the M/L ratio of groups (e.g., L04, Ramella et al. 2004), and in turn, the group M/L ratio is about an order of magnitude larger than for individual galaxies (e.g., Brinchmann & Ellis 2000). Remarkably, despite the fact that rich clusters are two orders of magnitude less efficient in converting baryons to stars than individual galaxies, their continually increasing M/L ratio with increasing mass suggests the possibility that they may still be slightly biased tracers of stellar mass in the universe. Unless the M/L vs. M_{200} relation flattens at the scale of $\sim 10^{15}$ $M_\odot$, the M/L ratio of clusters could be lower than the universal value. Unfortunately, there is no data for the K-band M/L ratio of superclusters to determine if the M/L ratio flattens at this size scale.

The mean M/L ratio for the clusters (corrected for passive evolution to $z = 0$) is 61.2 ± 1.8 $M_\odot/L_\odot$. Combining this with the luminosity density of the local universe measured by Kochanek et al. (2001) we find $\Omega_{m,0} = 0.22 \pm 0.02$ (random). This result is in good agreement with combined constraints from WMAP third-year results (WMAP3) and various other techniques (Spergel et al. 2006). The combined WMAP3 constraints on $\Omega_{m,0}$ range from a low-density of $\Omega_{m,0} = 0.226^{+0.030}_{-0.041}$ to a high-density of $\Omega_{m,0} = 0.299^{+0.019}_{-0.025}$. Interestingly, the measurement from the clusters is closest to the lowest density of the of preferred values from combined constraints. Previous studies using K-band M/L ratios of local clusters have also found values of $\Omega_{m,0}$ on the low-end of preferred values.

Both Rines et al. (2004) and Lin et al. (2003) measured $\Omega_{m,0}$ using their local cluster samples. Rines et al. found that the result depended strongly on the location in the clusters where the M/L ratio was measured. The cluster infall region had a lower M/L ratio than the virialized region and therefore they found $\Omega_{m,0} = 0.18 \pm 0.04$ from the virial region and $\Omega_{m,0} = 0.13 \pm 0.03$ from the infall region. Lin et al. (2003) performed the same analysis with a larger sample of 27 clusters. They found

$\Omega_{m,0} = 0.17 \pm 0.02$ using the mean M/L ratio of all clusters, and $\Omega_{m,0} = 0.19 \pm 0.03$ using a subsample of their most massive clusters.

Our analysis is in good agreement with both these studies, as well as the r-band measurement from the same clusters by Carlberg et al. (1997). Our results further confirm that $\Omega_{m,0}$ from clusters agrees well with concordance values but tends to be on the low-density end of preferred values. It is possible that the cluster measurements prefer lower $\Omega_{m,0}$ because their M/L ratios are still lower than the universal value. A measurement of the K-band M/L ratio on the supercluster scale would be a useful way to test this hypothesis. Regardless, the fact that the cluster $\Omega_{m,0}$ still agrees well with recent measurements of $\Omega_{m,0}$ using a variety of independent techniques, and combinations thereof suggests that the cluster M/L ratio is unlikely to be significantly lower than the universal value.

8. SUMMARY

We have presented the K-band scaling relations for 15 moderate-redshift clusters with extensive optical spectroscopy and wide-field K-band imaging. The cluster HON is well-correlated with M_{500} and T_x; however, the intrinsic scatter in the scaling relations at $z \sim 0.3$ is fairly large (37% and 46% respectively). Comparing to local clusters we find that the HON is consistent with no evolution at fixed cluster mass out to $z \sim 0.5$. This result, in tandem with the purely passive evolution of the cluster LF, and the fact that the cluster LF does not depend on mass suggests that if the significant tidal stripping of galaxy halos in clusters seen in numerical simulation occurs, the stellar mass within the halo is tightly bound and remains intact. This interpretation is further supported by recent SPH simulations which show that the baryonic matter is the amongst the most tightly bound mass within the halo.

Our data also show that both $L_{200,K}$ and $B_{gc,K}$ are well-correlated with the cluster dynamical mass and X-ray temperature. The slope of the L_{200} - M_{200} relation at $z \sim 0.3$ ($L_{200,K} \propto M_{200}^{0.83\pm0.11}$) is consistent with the slope measured for local clusters, suggesting that the cluster scaling relations are in place by at least $z \sim 0.3$. The good correlation, and relatively small scatter (intrinsic + measurement) in the $B_{gc,K}$ - M_{200} relation (35%) and $B_{gc,K}$ - T_x relation (25%) suggests that $B_{gc,K}$ would be useful mass indicator for upcoming cluster cosmology projects.

Our results from the M/L ratios of the clusters show that the moderate-redshift CNOC1 clusters are very similar to local clusters in that the M/L ratio is a slowly increasing function of cluster mass. By comparing the cluster M/L ratio to the local luminosity density we estimate that $\Omega_{m,0} = 0.22 \pm 0.02$, which agrees well with the original analysis of the CNOC1 clusters using optical data as well as with the local estimates using K-band photometry. The measured value is also in good agreement with recent WMAP third year joint constraints; however, similar to previous cluster studies the value is on the low-density end of preferred values.

The combined analysis of this paper and Paper I present a relatively simple picture of the evolution of the near-infrared properties of clusters from $z = 0$ to $z \sim 0.3$. The correlation between the cluster near-infrared properties (i.e., $L_{200,K}$, N_{500}, and $M_{200}/L_{200,K}$) and M_{200} shows no significant change between $z = 0$ and $z \sim 0.3$. Furthermore, the scatter in these scaling relations is similar at both redshifts. The cluster LF shows only passive evolution between $z = 0$ and $z \sim 0.3$ and does not depend on cluster mass. In addition to this, the (small) difference between the field and cluster LF at $z = 0$ is unchanged at $z \sim 0.3$. These results all show that there is little evolution in the the bulk of the stellar mass in cluster galaxies over this redshift range besides the passive aging of the stellar populations.

Specifically, it appears that 1) the significant tidal stripping of halo in high-density regions seen in N-body simulations does not affect the stellar mass contained in galaxies nor change the cluster scaling relations; 2) given passive evolution of the LF, and no-evolution in the HON, mergers and disruptions are unlikely to play a significant role in cluster galaxy evolution at $z < 0.3$; and 3) that the changes seen in the cluster stellar populations over the redshift interval $z = 0$ to $z \sim 0.3$ (i.e., the increase in blue-fraction/star-formation properties, and evolution of the morphology-density relation) are "superficial" - they result from changes in a small part of a galaxy's stellar mass, while the majority of the stellar mass is already in place and passively evolving.

Overall, it appears that the bulk of the stellar mass in cluster galaxies is in place, and evolving passively with few mergers or disruptions between $z \sim 0.3$ and $z = 0$, and that the the cluster scaling relations are produced by processes that occur at higher redshifts.

We thank the anonymous referee for a careful report which improved the clarity of this paper. A.M. would like to cite useful conversations and help from David Gilbank and Kris Blindert which significantly improved the quality of the data analysis. A. M. acknowledges financial support from the National Science and Engineering Research Council (NSERC) in the form of PGSA and PGSD2 scholarships. The research of H.K.C.Y. is supported by grants from Canada Research Chair Program, NSERC and the University of Toronto. P.H. acknowledges support from NSERC.

TABLE 1
Physical Properties of the CNOC1 Clusters

Cluster	z	σ_1 km s^{-1}	R_{200} Mpc	M_{200} $M_\odot \times 10^{14}$	T_x keV
(1)	(2)	(3)	(4)	(5)	(6)
A2390	0.2279	1095 ± 61	2.00	20.1 ± 3.4	$10.3^{+0.6}_{-0.6}$
MS0016+16	0.5466	1243 ± 128	1.89	24.0 ± 7.5	$9.2^{+1.0}_{-0.9}$
MS0302+16	0.4246	656 ± 93	1.07	3.7 ± 1.6	4^{+3}_{-1}
MS0440+02	0.1965	611 ± 62	1.13	3.5 ± 1.1	8^{+2}_{-1}
MS0451+02	0.2010	979 ± 76	1.81	15.0 ± 3.5	$6.1^{+0.7}_{-0.6}$
MS0451-03	0.5392	1354 ± 105	2.06	33.3 ± 7.6	$10.2^{+1.0}_{-1.0}$
MS0839+29	0.1928	788 ± 104	1.46	6.6 ± 2.7	$4^{+0.3}_{-0.3}$
MS1006+12	0.2605	912 ± 101	1.63	11.2 ± 3.8	7^{+1}_{-1}
MS1008-12	0.3062	1059 ± 107	1.85	17.2 ± 5.3	$5.9^{+0.9}_{-0.7}$
MS1224+20	0.3255	798 ± 90	1.38	7.5 ± 2.5	$4.3^{+0.65}_{-0.65}$
MS1231+15	0.2350	662 ± 69	1.20	4.5 ± 1.4	6^{+1}_{-1}
MS1358+62	0.3290	910 ± 54	1.57	12.0 ± 2.1	$8.0^{+1.1}_{-0.9}$
MS1455+22	0.2570	1169 ± 140	2.10	22.0 ± 8.2	$4.4^{+0.1}_{-0.1}$
MS1512+36	0.3726	697 ± 96	1.17	4.7 ± 2.0	$3.4^{+0.8}_{-0.7}$
MS1621+26	0.4274	833 ± 55	1.36	6.8 ± 1.4	7^{+3}_{-2}

TABLE 2
NIR Properties of the CNOC1 Clusters

Cluster	$L_{200,K}$ $L_\odot \times 10^{13}$	ϵ $L_{200,K}$ $L_\odot \times 10^{13}$	$(M/L)_{200,K}$	ϵ $(M/L)_{200,K}$	$B_{gc,K}$ $Mpc^{1.8}$	ϵ $B_{gc,K}$ $Mpc^{1.8}$	N_{500}	ϵ N_{500}
(1)	(2)	(3)	(4)	(5)	(6)	(7)	(8)	(9)
A2390	3.14	0.25	64	14	2302	303	338	50
MS0016+16	3.94	0.43	61	24	2298	311	389	56
MS0302+16	0.81	0.17	45	25	674	157	63	25
MS0440+02	1.63	0.43	21	8	1083	210	125	25
MS0451+02	2.40	0.29	63	18	1571	252	313	44
MS0451-03	2.79	0.08	119	34	2897	343	305	59
MS0839+29	0.79	0.14	83	43	1768	266	207	34
MS1006+12	1.96	0.18	57	24	2496	316	377	43
MS1008-12	2.64	0.28	65	28	1745	266	198	44
MS1224+20	1.34	0.27	56	24	733	169	139	32
MS1231+15	1.23	0.14	37	14	967	198	130	27
MS1358+62	3.05	0.25	39	8	1866	275	269	41
MS1455+22	2.03	0.37	108	50	982	199	89	46
MS1512+36	0.65	0.10	71	37	772	172	49	25
MS1621+26	2.47	0.15	27	7	1543	249	225	38

REFERENCES

Allen, S. W. 1998, MNRAS, 296, 392
Babbedge, T., et al. 2006, MNRAS, 370, 1159
Balogh, M., Morris, S. L., Yee, H. K. C., Carlberg, R. G., Ellingson, E. 1999, ApJ, 527, 54
Bell, E., McIntosh, D. H., Katz, N., & Weinberg, M. D. 2003, ApJS, 149, 289
Berlind, A. A., Blanton, M. R., Hogg, D. W., Weinberg, D. H., Davé, R., Eisenstein, D., Katz, N. 2005, ApJ, 629, 625
Berlind, A. A., et al. 2003, ApJ, 593, 1
Berlind, A. A., & Weinberg, D., 2002, ApJ, 575, 587
Blanton, M. R., et al. 2003, ApJ, 592, 819
Borgani, S., Girardi, M., Carlberg, R. G., Yee, H. K. C., Ellingson, E. 1999, ApJ, 527, 561
Brainerd, T. G., Specian, M. A., 2003, ApJ, 593, L7
Brinchmann, J., & Ellis, R. S. 2000, ApJ, 536, 77
Carlberg, R. G., Yee, H. K. C., Ellingson, E., Abraham R., Gravel, P., Morris, S. M., & Pritchet, C.J. 1996, ApJ, 462, 32
Carlberg, R. G., Yee, H. K. C., & Ellingson, E. 1997, ApJ, 478, 462
Cimatti, A., et al. 2002, A&A, 392, 395
Cole, S., et al. 2001, MNRAS, 326, 255
Cole, S., Lacey, C. G., Baugh, C. M., Frenk, C. S. 2000, MNRAS, 319, 168
Colín, P., Klypin, A. A., Kravtsov, A. V., Khokhlov, A. M. 1999, ApJ, 523, 32
Conroy, C., et al. 2005, ApJ, 635, 982
Cooray, A., & Sheth, R. 2002, Phys. Rep. 372, 1
Croft, R. A. C., et al. 2002, ApJ, 581, 20
Dahlen, T., et al. 2005, ApJ, 631, 126
De Propris, R., Stanford, S. A., Eisenhardt, P. R., Dickinson, M., Elston, R. 1999, AJ, 118, 719
Diaferio, A., Geller, M. J., Rines, K. J. 2005, ApJ 628, L97
Dressler, A., et al. 1997, Apj, 490, 577
Drory, N., et al. 2001, MNRAS, 325, 550
Eisenstein, D., Blanton, M., Zehavi, I., Bachall, N., Brinkmann, J., Loveday, J., Meiksin, A., Schneider, D. 2005, ApJ, 619, 178
Ellingson, E., Lin, H., Yee, H. K. C., & Carlberg, R. G. 2001, ApJ, 547, 609
Ellis, S., Jones, L. 2004, Proc. IAU Coll #195, astro-ph # 0405043
Elston, R. J. et al. 2006, ApJ, 639, 816
Fahlman, G., Kaiser, N., Squires, G., Woods, D. 1994, ApJ, 437, 56
Gardner, J. P., Cowie, L. L., Wainscoat, R. J. 1993, ApJL, 415, L9
Gavazzi, G., Pierini, D., Boselli, A., Tuffs, R. 1996, A&AS, 120, 489
Gilbank, D. G., Bower, R. G., Castander, F. J., Ziegler, B. L. 2004, MNRAS, 348, 551
Gladders, M. D., Yee, H. K. C., Majumdar, S., Barrientos, L. F., Hoekstra, H., Hall, P. B., Infante, L. 2006, astro-ph # 0603588
Gioia, I. M., Maccaraco, T., Schild, R. E., Wolter, A., Stocke, J. T., Morris, S. L., Henry, J. P. 1990, ApJSS, 72, 567
Halkola, A., Seitz, S., Pannella, M. 2006, astro-ph # 0611078
Hansen, S. M., McKay, T. A., Wechsler, R. H., Annis, J., Sheldon, E. S., Kimball, A. 2005, ApJ, 633, 122
Henry, J. P. 2000, ApJ, 534, 565
Hoekstra, H., Hsieh, B. C., Yee, H. K. C., Lin, H., Gladders, M. D. 2005, ApJ, 635, 73
Hoekstra, H., van Waerbeke, L., Gladders, M. D., Mellier, Y., Yee, H. K. C. 2002, ApJ, 577, 604
Hoekstra, H., Franx, M., Kuijken, K., Squires, G. 1998, 504, 636
Hicks, A., Ellingson, E., Hoekstra, H., Yee, H. K. C. 2006, ApJ, in-press
Ilbert, O., et al. 2005, A&A, 439, 863
Kim, T.-S., Carswell, R. F., Cristiani, S., D'Odorico, S., Giallongo, E. 2002, MNRAS, 335, 555
Kochanek, C. S., White, M., Huchra, J., Macri, L., Jarrett, T. H., Schneider, S. E., Mader, J. 2003, ApJ, 585, 161
Kochanek, C. S., et al. 2001, ApJ, 560, 566
Kodama, T., & Bower, R. 2003, MNRAS, 346, 1
Kosowsky, A. 2006, New Astron. Rev., 50, 969
Kravtsov, A. V., Berlind, A. A., Wechsler, R. H., Klypin, A. A., Gottlöber, S., Allgood, B., Primack, J. R. 2004, 609, 35
Lewis, A. D., Ellingson, E., Morris, S. L., Carlberg, R. G. 1999, ApJ, 517, 587
Lima, M., & Hu, W., 2005, Phys. Rev. D., 72, 043006
Lin, H., Yee, H. K. C., Hall, P. B., Hsieh, B. C. 2007, in-preparation
Lin, Y.-T., Mohr, J. J., Gonzalez, A. H., & Stanford, S. A. 2006, ApJL, in-press
Lin, Y.-T., Mohr, J. J., & Stanford, S. A. 2004, ApJ, 610, 745 (L04)
Lin, Y.-T., Mohr, J. J., & Stanford, S. A. 2003, ApJ, 591, 749
Longair, M. S., & Seldner, M. 1979, MNRAS, 189, 433
Luppino, G. A., & Gioia, I. M. 1995, 445, 77
Maihara, T., et al. 2001, PASJ, 53, 25
Mandelbaum, R., Seljak, U., Kauffmann, G., Hirata, C. M., Brinkmann, J. 2006, MNRAS, 368, 715
Mannucci, F., Basile, F., Poggianti, B. M., Cimatti, A., Daddi, E., Pozzetti, L., Vanzi, L. 2001, MNRAS, 326, 745
McDonald, P., et al. 2006, ApJS, 163, 80
Miller, C. J., et al. 2005, AJ, 130, 968
Mushotzky, R. F., & Scharf, C. A. 1997, ApJL, 482, L13
Muzzin, A., Yee, H. K. C., Hall, P. B., Ellingson, E., & Lin, H. 2006, ApJ, accepted, astro-ph # 0612202
Mohr, J. J. 2004, astro-ph # 0408484
Nagai, D., & Kravtsov, A. 2005, ApJ, 618, 557
Nakamura, O., et al. 2003, AJ, 125, 1682
Natarajan, P., Kneib, J.-P., Smail, I. 2002, ApJ, 580, L11
Navarro, J. F., Frenk, C. S., White, S. D. M. 1997, ApJ, 490, 493
Norberg, P., et al. 2002, MNRAS, 332, 827
Norberg, P., et al. 2001, MNRAS, 328, 64
Oort, J. H., 1958, in La Structure et L'Évolution de L'Univers, Onzieme Conseil de Physique, ed. R. Stoops (Brussels: Solvay Institute), 163
Pearce, F. R., et al. 2001, MNRAS, 326, 649
Pierre, M., Le Borgne, J. F., Soucail, G., Kneib, J. P. 1996, A&A, 311, 413
Poggianti, B. M., Smail, I., Dressler, A., Couch, W. J., Barger, A. J., Butcher, H., Ellis, R. S., Oemler, A. 1999, ApJ, 518, 576
Poggianti, B. M. 1997, A & AS, 122, 399
Pozzetti, L., et al. 2003, A&A, 402, 837
Press, W. H., Tuekolsky, S. A., Vetterling, W. T., Flannery, B. P. 1992, Numerical Recipes in Fortran 77, Vol 1; Second Edition; Cambridge, Cambridge University Press
Ramella, M., Boschin, W., Geller, M. J., Mahdavi, A., Rines, K. 2004, AJ, 128, 2022
Rines, K., Geller, M. J., Diaferio, A., Kurtz, M. J., Jarrett, T. H. 2004, AJ, 128, 1078 (R04)
Rix, H.-W., Rieke, M. J. 1993, ApJ, 418, 123
Ruhl, J. et al. 2004, in Astronomical Structures & Mechanisms Technology. Edited by Antebi, Joseph; Lemke, Dietrich, Proceedings of the SPIE, Volume 5498, pp.11
Saracco, P., et al. 2001, A&A, 375, 1
Seljak, U., et al. 2005, Phys. Rev. D., 71, 043511
Sheldon, E. S., et al. 2004, AJ, 127, 2544
Skrutskie, M. F., et al. 2006, AJ, 131, 1163
Spergel, D. N., et al. 2006, astro-ph # 0603449
Smail, I., Ellis, R. S., Dressler, A., Couch, W. J., Oemler, A., Sharples, R. M., Butcher, H. 1997, ApJ, 479, 70
Smail, I., Ellis, R. S., Fitchett, M. J., Edge, A. C. 1995, MNRAS, 273, 277
Stanford, S. A., Eisenhardt, P. R., Dickinson, M., Holden, B. P., de Propris, R. 2002, ApJS, 142, 153
Strazzullo, V., et al. 2006, A&A, 450, 909
Tasitsiomi, A., Kravtsov, A. V., Wechsler, R. H., Primack, J. R. 2004, ApJ, 614, 533
Tinker, J. L., Weinberg, D. H., Zheng, Z., Zehavi, I. 2005, ApJ, 631, 41
Toft, S., Mainieri, V., Rosati, P., Lidman, C., Demarco, R., Nonino, M., Stanford, S. A. 2004, A&A, 422, 29
Treu, T., Koopmans, L. V., Bolton, A. S., Burles, S., Moustakas, L. A. 2006, ApJ, 640, 662
van der Marel, R. P., Magorrian, J., Carlberg, R. G., Yee, H. K. C., Ellingson, E. 2000, AJ, 119, 2038
Weinberg, D. H., Colombi, S., Romeel, D., Katz, N. 2006, astro-ph#0604393
Weinberg, D. H., Davé, R., Katz, N., Hernquist, L. 2004, ApJ, 601, 1
Wolf, C., Meisenheimer, K., Rix, H.-W., Borch, A., Dye, S., Kleinheinrich, M. 2003, A&A, 401, 73
Wu, X.-P. 2000, MNRAS, 316, 299
Yee, H. K. C., Gladders, M. D., Gilbank, D. G., Majumdar, S., Hoekstra, H., Ellingson, E., 2007, astro-ph#0701839
Yee, H. K. C., & Ellingson, E. 2003, ApJ, 585, 215

Yee, H. K. C., et al. 2000, ApJS, 129, 475
Yee, H. K. C., & Lopez-Cruz, O., AJ, 117, 1985
Yee, H. K. C., Ellingson, E., & Carlberg, R. G. 1996, ApJS, 102, 269
Yee, H. K. C. 1991, PASP, 103, 662
Yoshikawa, K., Taruya, A., Jing, Y. P., Suto, Y. 2001, ApJ, 558, 520
Zehavi, I., et al. 2005a, ApJ, 630, 1
Zehavi, I., et al. 2005b, ApJ, 621, 22
Zhu, G., Zheng, Z., Lin, W. P., Jing, Y. P., Kang, X., Gao, L. 2006, ApJ, 639, L5